
SimAD: A Simple Dissimilarity-based Approach for Time Series Anomaly Detection

Zhijie Zhong

South China University of Technology
Guangzhou, China
csemor@mail.scut.edu.cn

Zhiwen Yu

South China University of Technology
Guangzhou, China
zhwyu@scut.edu.cn

Xing Xi

South China University of Technology
Guangzhou, China
202311089252@mail.scut.edu.cn

Yue Xu

South China University of Technology
Guangzhou, China
202164700172@mail.scut.edu.cn

Jiahui Chen

Guangdong University of Technology
Guangzhou, China
csjhchen@gmail.com

Kaixiang Yang*

South China University of Technology
Guangzhou, China
yangkx@scut.edu.cn

Abstract

Despite the prevalence of reconstruction-based deep learning methods, time series anomaly detection remains challenging. Existing approaches often struggle with limited temporal contexts, inadequate representation of normal patterns, and flawed evaluation metrics, hindering their effectiveness in identifying aberrant behavior. To address these issues, we introduce **SimAD**, a **Simple** dissimilarity-based approach for time series **Anomaly Detection**. SimAD incorporates an advanced feature extractor adept at processing extended temporal windows, utilizes the EmbedPatch encoder to integrate normal behavioral patterns comprehensively, and introduces an innovative ContrastFusion module designed to accentuate distributional divergences between normal and abnormal data, thereby enhancing the robustness of anomaly discrimination. Additionally, we propose two robust evaluation metrics, UAff and NAff, addressing the limitations of existing metrics and demonstrating their reliability through theoretical and experimental analyses. Experiments across **seven** diverse time series datasets demonstrate SimAD's superior performance compared to state-of-the-art methods, achieving relative improvements of **19.85%** on F1, **4.44%** on Aff-F1, **77.79%** on NAff-F1, and **9.69%** on AUC on six multivariate datasets. Code and pre-trained models are available at <https://github.com/EmorZz1G/SimAD>.

1 Introduction

Time series anomaly detection is essential in time series analysis, aiming to identify abnormal patterns within time series data and accurately determine their locations [1, 2]. Previous studies have predominantly concentrated on addressing this issue using unsupervised approaches based on reconstruction [3]. These approaches assume the models have been trained perfectly on normal data and assign higher anomaly scores to the anomalous data during the testing phase.

*Corresponding author

However, these methods have shown insufficient performance in practical applications. Reviewing existing research [4, 5, 6, 7] and conducting comprehensive experiments (See the analyses in our experiments), we have identified several significant challenges in the time series anomaly detection field. **Challenge 1:** Solely relying on reconstruction is inadequate for enhancing the detection capability of the models [8, 4]. Many methods depend solely on the reconstruction assumption; however, this approach is frequently inadequate. We have further substantiated this through our experiments, employing sensitivity and ablation analyses. **Challenge 2:** Inadequate utilization of extended time windows. The complexity of the original attention mechanism has restricted previous methods, often confining the window length to 200 or less [8, 9]. Consequently, this limitation impedes the capturing of more informative data. **Challenge 3:** Restricted expressive power in representing normal features. On one hand, certain methods fail to model normal or abnormal data (or both) in a targeted manner. On the other hand, most models suffer from a restricted number of parameters, thereby limiting their expressive power.

To address the aforementioned challenges, we propose a **simple** dissimilarity-based approach for time series Anomaly Detection (**SimAD**). SimAD applies to both univariate and multivariate real-world data. To tackle **Challenge 1**, we have developed a Feature Extractor capable of accommodating longer time windows, which is achieved by dividing the sequence into multiple patches, enabling SimAD to learn extended temporal receptive fields while utilizing fewer parameters. To address **Challenges 2** and **3**, we incorporate the prototype into the attention mechanism at each layer. Additionally, we propose the EmbedPatch Encoder to enhance the representation capability of normal features. Furthermore, we introduce the ContrastFusion module, which amplifies the distribution differences between normal and abnormal data.

Furthermore, we have conducted an analysis of the limitations associated with existing evaluation methods. These limitations have resulted in false perceptions regarding the progress made in the time series anomaly detection [10, 11, 12]. To enable a fair comparison of the performance among various methods, we propose two enhanced evaluation metrics: UAff and NAff. We have undertaken analyses from both theoretical and experimental perspectives to establish the reliability of these newly proposed metrics. Our approach demonstrates a significant out-performance through extensive experimental validation compared to the current state-of-the-art (SOTA) methods in the time series anomaly detection task.

In summary, our paper makes the following contributions:

- (1) We propose a novel and effective algorithm, **SimAD**, for long-term time series anomaly detection, capable of supporting longer time window sizes.

- (2) We introduce improved anomaly detection evaluation metrics, **UAff** and **NAff**, and provide theoretical and experimental analyses to demonstrate their reliability.

- (3) Our algorithm outperforms significantly the current state-of-the-art methods on real-world datasets (See Figure 1). Moreover, we have publicly made our code and models available for further research.

2 Related work

Unsupervised methods have received considerable attention, given the scarcity of labeled data for anomaly detection in time series sequences. Broadly, these methods can be categorized as: (1) Algorithms based on classical machine learning, such as [13, 14], transform traditional machine learning approaches into deep neural network structures, enhancing their ability to handle complex data. (2) Reconstruction-based approaches, exemplified by [15, 9, 16], involve training models using normal data and leveraging reconstruction error as an anomaly score, attributing higher scores to anomalous data during testing. (3) Prediction-based techniques, as demonstrated by [17], learn from historical data to predict future observations, considering prediction errors as the foundation for anomaly detection. (4) Generative adversarial learning, such as [18, 19, 20], utilizes generative models to learn the distribution of normal data and a discriminator network to detect anomalies.

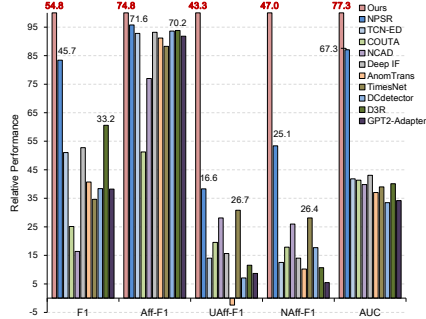


Figure 1: Comparison analysis. The vertical axis shows relative performance, and data labels reflect the models’ authenticity scores.

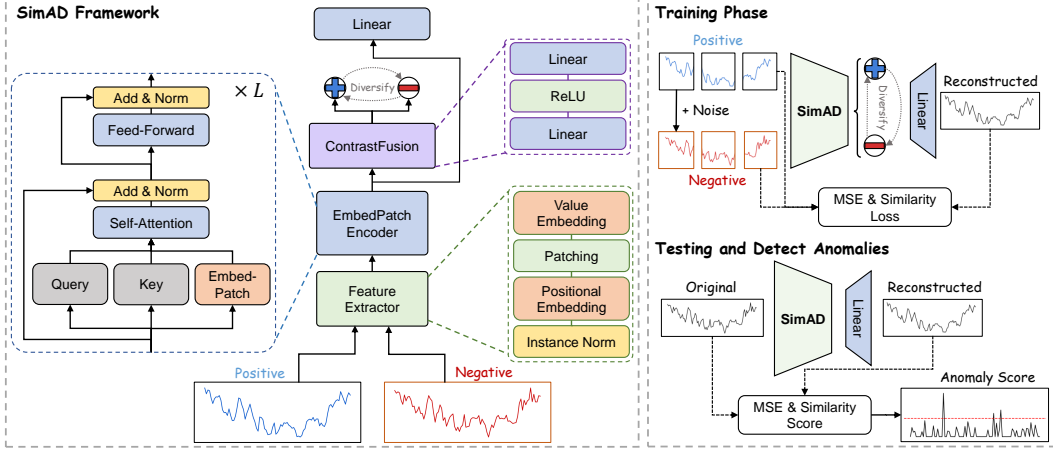


Figure 2: The framework and workflow of SimAD.

In recent years, some innovative algorithms have emerged in the field of anomaly detection, including: (1) Transformer-based approaches [8, 21, 22] utilize Transformer models that have demonstrated remarkable success in natural language processing tasks applied to anomaly detection. (2) Contrastive learning-based methods [23, 24, 25, 26, 27] employ contrastive learning techniques to acquire robust representations for anomaly detection. (3) Diffusion-based techniques [28, 29] utilize diffusion processes to capture the propagation of anomalies in complex networks and time series sequences. (4) Large Language Models (LLMs) [30] employ state-of-the-art language models, such as GPT-2, adapted for anomaly detection tasks, leveraging their advanced network architectures and knowledge representation capabilities.

These algorithms can be considered extensions or variations of the categories above. They incorporate more advanced network structures and knowledge representation methods to enhance anomaly detection performance.

However, the existing methods have not effectively addressed the three main challenges we summarized. Most methods are limited by a few learnable parameters, which restricts their ability to capture long-term dependencies in the data. Moreover, some reconstruction-based methods solely focus on the task of reconstruction, which is considered a limitation.

3 Proposed Approach

In the context of a temporal anomaly detection task, the input $\mathbf{X} \in \mathbb{R}^{T \times C}$, where T represents the length of the time series and C denotes the number of channels. The goal of this task is to predict the corresponding labels $y \in \mathbb{R}^T$, where a value of $y_i = 1$ indicates an anomaly at the i th time point.

3.1 Overview

This section introduces SimAD, as depicted in Figure 2. SimAD comprises a Feature Extractor, EmbedPatch Encoder, and ContrastFusion module. Firstly, the original time series data \mathbf{X} undergoes processing by the Feature Extractor to obtain patch tokens \mathbf{N} . Subsequently, at each layer of the EmbedPatch Encoder, the EmbedPatch attention mechanism merges the patch tokens from the previous layer with the tokens themselves, capturing their interdependencies. Finally, we utilize a single linear layer to reconstruct the original features and compute anomaly scores. Additionally, we design the ContrastFusion module to enhance the discriminative power between normal and abnormal data distributions, thereby improving the overall detection performance.

3.2 Feature Extractor

First, the original time series data \mathbf{X} is fed to the feature extractor. To address distribution shifts [31, 32], we introduce Instance Normalization (IN). Then, the improved Positional Embedding (PE)

is employed to incorporate temporal positional encoding without channel encoding, enabling SimAD to learn the relationships between channels actively. The Patching operation involves dividing \mathbf{X}' into multiple (N) patches of length P ($\mathbf{N}' \in \mathbb{R}^{N \times P \times C}$) and rearranging them as $\mathbf{N}' \in \mathbb{R}^{N \times (P \cdot C)}$. Conversely, VE refers to a simple linear transformation that maps all the patches into a unified space, $\mathbf{N} \in \mathbb{R}^{N \times D}$. The processing performed by the Feature Extractor can be described as follows:

$$\begin{aligned}\mathbf{X}' &= \text{PE}(\text{IN}(\mathbf{X})), \\ \mathbf{N} &= \text{VE}(\text{Patching}(\mathbf{X}')).\end{aligned}\tag{1}$$

Thanks to the designed feature extractor, SimAD can handle data with longer time windows. Our experiments have shown the necessity of using longer windows.

3.3 EmbedPatch Encoder

To enhance SimAD's ability to memorize normal samples and improve its generalization capability, we have made a simple improvement to the original attention model. This improvement involves incorporating the EmbedPatch $\mathbf{E}^{(i)} \in \mathbb{R}^{V \times D}$ with embedded queries into the backbone of SimAD, drawing inspiration from [4, 6, 7]. Here, V represents the number of patch embeddings in SimAD. Determining the appropriate value for V often requires prior knowledge and a larger number of embeddings to accommodate different scenarios [33]. Therefore, a linear projection is applied after EmbedPatch, resulting in $\mathbf{E}^{(i)'} \in \mathbb{R}^{N \times D}$, where $N \ll V$, to reduce the dimensionality. This simple component enables SimAD to efficiently learn relevant information from normal samples without relying solely on prior knowledge.

To achieve this, we employ an improved multi-head attention layer. For each head $k = \{1, 2, \dots, U\}$, we define the query matrix as $\mathbf{Q}_k^{(i)} = \mathbf{N}^{(i)} \mathbf{W}_k^Q$, the key matrix as $\mathbf{K}_k^{(i)} = \mathbf{N}^{(i)} \mathbf{W}_k^K$, and the value matrix as $\mathbf{V}_k^{(i)} = \mathbf{W}_k^V \mathbf{E}^{(i)'}$. Here, $\mathbf{W}_k^Q, \mathbf{W}_k^K \in \mathbb{R}^{d \times d}$, $\mathbf{W}_k^V \in \mathbb{R}^{N \times V}$, and d is defined as $\lfloor \frac{D}{U} \rfloor$. Next, we define the attention calculation between different patches in each layer as follows:

$$\mathbf{Z}_k^{(i)} = \text{Attention}(\mathbf{Q}_k^{(i)}, \mathbf{K}_k^{(i)}, \mathbf{V}_k^{(i)}) = \text{Softmax}\left(\frac{(\mathbf{Q}_k^{(i)} \mathbf{K}_k^{(i)\top})}{\sqrt{d}} \mathbf{V}_k^{(i)}\right).\tag{2}$$

At the end of each layer, we utilize a linear layer to aggregate the features $\mathbf{Z}_k^{(i)}$ from different heads, resulting in $\mathbf{Z}^{(i)} \in \mathbb{R}^{N \times D}$. Subsequently, we proceed with the original "Add & Norm" operation to generate the input, $\mathbf{N}^{(i+1)}$, for the next layer.

$$\begin{aligned}\mathbf{N}^{(i)'} &= \text{LayerNorm}(\mathbf{N}^{(i)} + \mathbf{Z}^{(i)}), \\ \mathbf{N}^{(i+1)} &= \text{LayerNorm}(\mathbf{N}^{(i)'} + \text{FFN}(\mathbf{N}^{(i)'})),\end{aligned}\tag{3}$$

where $\text{FFN}(\cdot)$ represents a multi-layer feed-forward network. Finally, a simple fully connected layer is used to restore $\mathbf{Z}^{(L)}$ to $\hat{\mathbf{X}}$ from the last layer. During the training phase, the Mean Square Error (MSE) is used to measure the difference between \mathbf{X} and $\hat{\mathbf{X}}$, and a patch-based similarity loss is employed to ensure continuity between patches. During the testing phase, SimAD utilizes \mathcal{L}_{rec} to calculate anomaly scores and detect anomalies.

$$\mathcal{L}_{rec} = \text{MSE}(\hat{\mathbf{X}}, \mathbf{X}) + (1 - \text{Similarity}(\hat{\mathbf{X}}, \mathbf{X})).\tag{4}$$

In the implementation, we utilize patch-based cosine similarity as a similarity measure.

3.4 ContrastFusion module

While the EmbedPatch Encoder enables SimAD to memorize normal samples, it does not substantially enhance the discrimination between normal and abnormal samples. To address this limitation, we have developed the ContrastFusion module using contrastive learning inspired by [34]. This module aims to increase the distance between normal and abnormal data features, thereby improving the precision of detection.

To generate negative samples for contrastive learning without introducing excessive prior knowledge, we employ the simplest method of generating negative samples using Gaussian noise. Specifically,

we use the equation $\mathbf{X}_n = \mathbf{X} + \alpha \cdot \mathbf{J}$, where \mathbf{J} is sampled from a standard Gaussian distribution, and α is employed to control the level of noise.

Drawing inspiration from previous work on denoising autoencoders [35], we integrate a denoising loss into the final objective function.

$$\mathcal{L}_{denoise} = \text{MSE}(\hat{\mathbf{X}}_n, \mathbf{X}) + (1 - \text{Similarity}(\hat{\mathbf{X}}_n, \mathbf{X})). \quad (5)$$

To efficiently and expeditiously learn invariant features, we concurrently feed both the positive sample \mathbf{X} and the negative sample \mathbf{X}_n into the Feature Extractor and EmbedPatch Encoder, resulting in the acquisition of the hidden feature representations \mathbf{N} and \mathbf{N}_n . For this purpose, we utilize a projection head $\mathcal{P}(\cdot)$, akin to prior contrastive learning methods, to facilitate the acquisition of meaningful and discriminative representations.

$$\mathbf{H} = \mathcal{P}(\mathbf{N}) = \text{FC}(\text{ReLU}(\text{FC}(\mathbf{N}))). \quad (6)$$

Afterwards, we derive low-dimensional hidden representations \mathbf{H} and \mathbf{H}_n for \mathbf{N} and \mathbf{N}_n respectively. To design an asymmetric feature contrastive loss, we utilize gradient stopping.

$$\begin{aligned} \mathcal{L}_{cont} = & \text{MSE}(\mathbf{H}, \text{StopGrad}(\mathbf{H}_n)) + (1 - \text{Similarity}(\mathbf{H}, \text{StopGrad}(\mathbf{H}_n))) \\ & + \text{MSE}(\mathbf{H}_n, \text{StopGrad}(\mathbf{H})) + (1 - \text{Similarity}(\mathbf{H}_n, \text{StopGrad}(\mathbf{H}))). \end{aligned} \quad (7)$$

3.5 Joint Optimization

As outlined in the preceding sections, SimAD strives to optimize the reconstruction of positive samples, denoise noisy samples, and maximize the feature disparities between positive and negative samples. During the initial stages of training, the model focuses primarily on reconstruction and denoising, with the contrastive loss introducing additional training complexity. Thus, in the initial $N_{\text{warm-up}}$ iterations, the weight of the contrastive loss incrementally rises with each iteration until it reaches the maximum value of β_{\max} : $\beta_i = \min\{\frac{i+1}{N_{\text{warm-up}}}, \beta_{\max}\}$. The final objective function combines the reconstruction loss, denoising loss, and contrastive loss. It can be represented as follows:

$$\mathcal{L} = \mathcal{L}_{rec} + \mathcal{L}_{denoise} - \beta \mathcal{L}_{cont}. \quad (8)$$

3.6 Improving Affiliation metrics

In recent studies [10, 11, 12], researchers have highlighted the limitations of conventional metrics used in time-series anomaly detection. The Affiliation metric [36] is a parameter-free method that has demonstrated promising performance across various aspects. However, based on experiments and theoretical analysis (refer to the appendix), we illustrate that when confronted with random anomaly scores, the Affiliation precision (Aff-Pre) tends to approach 0.5. In contrast, the Affiliation recall (Aff-Rec) tends to approach 0.99, leading to an Affiliation F1 score (Aff-F1) of approximately 0.7, which suggests that the discriminatory capability of this metric is inadequate. To overcome this limitation, we introduce enhanced Unbiased Affiliation (UAff) and Normalized Affiliation (NAff) metrics. Our metrics exhibit superior discriminatory ability and provide a more accurate reflection of the algorithm’s precision performance.

Based on our experimental findings (refer to Table 4 in the appendix), we have observed that the Affiliation precision (Aff-Pre) varies across different datasets but consistently tends to approach 0.5, which can be interpreted as an indicator of dataset-specific bias, which we denote as $\mathbf{Aff-Pre}_{bias}$. Simultaneously, there has been insufficient encouragement for high-precision models, while the penalties for low-precision models are inadequate. We introduce unbiased metrics called Unbiased Affiliation precision (UAff-Pre) and Unbiased Affiliation F1 (UAff-F1) to tackle this issue. These metrics aim to alleviate the dataset-specific bias and offer a more equitable assessment of the algorithm’s precision performance.

$$\mathbf{UAff-Pre} = \frac{\mathbf{Aff-Pre} - \mathbf{Aff-Pre}_{bias}}{1 - \mathbf{Aff-Pre}_{bias}} \quad (9)$$

$$\mathbf{UAff-F1} = \frac{2 \cdot |\mathbf{UAff-Pre}| \cdot \mathbf{Aff-Rec}}{|\mathbf{UAff-Pre}| + \mathbf{Aff-Rec}} \cdot (-1)^{|\mathbf{UAff-Pre} < 0|}. \quad (10)$$

Here, $(-1)^{|\mathbf{UAff-Pre}<0|}$ indicates **UAff-F1** is negative when **UAff-Pre** < 0 . While **UAff-Pre** represents an improvement over its original version and surpasses **UAff-F1**, it does introduce additional parameters, thereby deviating from its parameter-free nature. However, we have observed that the majority of real-world datasets exhibit $\mathbf{Aff-Pre}_{bias} \leq 0.55$. Therefore, we propose a modified version of the NAff metrics. The computation process follows a similar formula as mentioned earlier, with the exception that we set $\mathbf{Aff-Pre}_{bias}$ to 0.5 while maintaining other aspects unchanged. In other words, **NAff-Pre** can be calculated as $2 \cdot (\mathbf{Aff-Pre} - 0.5)$. The mathematical analysis of the metrics is shown in the appendix.

4 Experiments

4.1 Experimental settings

We evaluate SimAD using six real-world datasets: MSL, SMAP, PSM, SWaT, WADI, and Swan. Additionally, we utilize a univariate dataset, UCR [37]. The details of these datasets are described in Table 4 in the appendix. Similarly, the implementation details and pseudo-code of the algorithm can also be found in the appendix.

4.2 Baselines

Our model is compared against 12 baseline models, which include machine learning-enhanced algorithms such as Deep SVDD [13] and Deep Isolation Forest (Deep IF) [14]; reconstruction-based approaches like USAD [15], TCN-ED [9] and NPSR [38]; prediction-based methods like TimesNet [17]; Transformer-based models such as Anomaly Transformer (AnomTrans) [8] and TranAD [22]; contrastive learning-based models like COUTA [23], NCAD [24], and DCdetector [25]; diffusion-based model D3R [28]; and LLM-based model GPT2-Adapter [30].

4.3 Metrics

We employ the F1 score without point adjustment, the original Aff-F1 score, and our improved UAff-F1 and NAff-F1 scores for performance evaluation. We completely exclude the point-adjusted F1 score due to its acknowledged drawbacks and potential for false improvements. It is important to note that the classical F1 score is not optimal for time series data; however, it can still be employed for evaluation purposes [10], as detailed in our appendix. Furthermore, we present the AUC scores for all datasets (Table 3).

4.4 Quantified comparisons

Table 3 presents a performance comparison between the SimAD model and multiple baseline models using six real-world datasets. Overall, SimAD performs superior to other models in most evaluation metrics, particularly on the SWaT, WADI, and Swan datasets. Specifically, compared to the best baseline models on each dataset, SimAD exhibits absolute improvements of **5.15%** (76.88%→82.03%), **13.31%** (50.67%→63.98%), and **15.24%** (55.99%→71.23%) in F1 score. In contrast, the NAff-F1 score exhibits absolute improvements of **11.09%** (55.73%→66.82%), **30.87%** (45.39%→76.26%), and **19.05%** (33.99%→53.04%) respectively.

The MSL and SMAP datasets are composed of multiple concatenated sub-datasets rather than continuous ones, which has resulted in SimAD not being able to establish a larger gap compared to other algorithms.

Table 1 summarizes the evaluation metric scores of the models across all datasets, clearly indicating that SimAD achieved absolute improvements of **9.07%** on F1, **3.18%** on Aff-F1, **16.63%** on UAff-F1, and **20.55%** on NAff-F1, and **6.83%** AUC compared to the SOTA model.

In contrast, models such as TimesNet and D3R exhibit good performance on specific evaluation metrics

Table 1: The average performance and ranking of different algorithms. **RK.** represents the ranking of the corresponding metric.

| Avg. | F1 | RK. | Aff-F1 | RK. | UAff-F1 | RK. | NAff-F1 | RK. | AUC | RK. | Avg.RK. |
|--------------|--------------|----------|--------------|----------|--------------|----------|--------------|----------|--------------|----------|----------|
| Random | 26.62 | 8 | 69.21 | 7 | 0.00 | 14 | 11.51 | 10 | 50.10 | 15 | 10.8 |
| Deep SVDD | 27.26 | 7 | 65.15 | 12 | 7.73 | 10 | 7.34 | 13 | 70.44 | 2 | 8.8 |
| USAD | 27.57 | 6 | 65.06 | 13 | 7.33 | 12 | 6.97 | 14 | 65.58 | 5 | 10 |
| TCN-ED | 27.96 | 5 | 69.41 | 6 | 12.16 | 8 | 11.76 | 9 | 64.61 | 6 | 6.8 |
| COUTA | 13.77 | 14 | 38.32 | 15 | 16.93 | 4 | 16.77 | 5 | 63.87 | 8 | 9.2 |
| TranAD | 26.54 | 9 | 67.37 | 10 | 13.88 | 6 | 13.55 | 7 | 64.41 | 7 | 7.8 |
| NCAD | 8.97 | 15 | 57.57 | 14 | 24.35 | 3 | 24.38 | 4 | 61.55 | 10 | 9.2 |
| Deep IF | 28.90 | 4 | 69.69 | 5 | 13.57 | 7 | 13.18 | 8 | 66.56 | 4 | 5.6 |
| AnomTrans | 22.30 | 10 | 68.17 | 9 | -2.11 | 15 | 9.58 | 12 | 57.20 | 12 | 11.6 |
| TimesNet | 18.98 | 13 | 66.02 | 11 | 26.68 | 2 | 26.41 | 2 | 60.27 | 11 | 7.8 |
| DCdetector | 21.03 | 11 | 70.01 | 4 | 6.14 | 13 | 16.61 | 6 | 51.72 | 14 | 9.6 |
| D3R | 33.19 | 3 | 70.16 | 3 | 10.00 | 9 | 10.02 | 11 | 62.01 | 9 | 7 |
| GPT2-Adapter | 20.95 | 12 | 68.67 | 8 | 7.49 | 11 | 5.11 | 15 | 52.84 | 13 | 11.8 |
| NPSR | 45.71 | 2 | 71.60 | 2 | 16.58 | 5 | 25.07 | 3 | 67.26 | 3 | 3 |
| Ours | 54.79 | 1 | 74.78 | 1 | 43.31 | 1 | 46.96 | 1 | 77.27 | 1 | 1 |

(UAff-F1, Aff-F1). Still, their performance on other metrics (Aff-F1, NAff-F1) is inferior to that of SimAD but even lower than that of random algorithms. Figure 1 visually illustrates the substantial advantages of our model compared to other baseline models across multiple evaluation metrics, which further confirms the superior generalization capability of SimAD, whereas other algorithms may display larger performance fluctuations due to an excessive focus on specific dataset characteristics.

In evaluating the univariate dataset UCR, SimAD also demonstrates superior performance compared to other models. Table 2 presents the specific metric scores of SimAD and baseline models, including Avg.+ (calculated using only positive values) and Avg. scores. SimAD achieves an absolute improvement of **13.33%** (1.66% \rightarrow 14.99%) in **Avg.+ F1** score and **13.38%** (1.61% \rightarrow 14.99%) in **Avg. F1** score compared to the best baseline model. Furthermore, SimAD achieves an absolute improvement of **25.75%** (9.41% \rightarrow 35.16%) in **Avg.+ UAff-F1** score and **17.52%** (2.01% \rightarrow 19.53%) in **Avg. UAff-F1** score compared to the best baseline model.

Table 3: Comparison results. All results are in %, the best in **Bold**, and the second in underlined.

| Datasets | MSL | | | | | | | | SMAP | | | | | | | | SWaT | | | | | | | |
|--------------|--------------|--------------|---------|---------|--------------|--------------|--------------|--------------|--------------|-------|---------|--------------|--------------|--------------|--------------|--------------|-------|-------|--------------|--------------|--------------|---------|---------|---------|
| | F1 | AUC | Aff-Pre | Aff-Rec | Aff-F1 | UAff-F1 | NAff-F1 | NAff-F1 | F1 | AUC | Aff-Pre | Aff-Rec | Aff-F1 | UAff-F1 | NAff-F1 | NAff-F1 | F1 | AUC | Aff-Pre | Aff-Rec | Aff-F1 | UAff-F1 | NAff-F1 | NAff-F1 |
| Random | 18.60 | 50.01 | 51.34 | 99.99 | 67.84 | 0.00 | 5.20 | 22.06 | 50.18 | 51.48 | 100.0 | 67.97 | 0.00 | 5.74 | 21.06 | 50.10 | 52.94 | 99.99 | 69.23 | 0.00 | 11.09 | | | |
| Deep SVDD | <u>24.30</u> | 61.80 | 52.67 | 99.93 | 68.98 | 10.53 | 10.13 | 8.91 | 61.14 | 44.98 | 88.45 | 59.64 | -17.60 | -18.02 | 22.57 | 86.81 | 53.58 | 99.99 | 69.77 | 13.75 | 13.37 | | | |
| USAD | 22.50 | 57.12 | 51.90 | 97.29 | 67.69 | 7.73 | 7.31 | 9.84 | 62.79 | 39.56 | 69.48 | 50.41 | -31.78 | -32.12 | 21.70 | 88.66 | 53.00 | 100.0 | 69.28 | 11.71 | 11.31 | | | |
| TCN-ED | 19.66 | 51.14 | 51.44 | 99.99 | 67.93 | 6.04 | 5.61 | 22.90 | 58.91 | 51.39 | 99.98 | 67.89 | 5.86 | 5.42 | 21.65 | 89.23 | 52.98 | 100.0 | 69.26 | 11.64 | 11.24 | | | |
| COLTA | 20.88 | 55.59 | 51.24 | 99.65 | 67.68 | 5.29 | 4.85 | 22.69 | 58.74 | 51.48 | 100.0 | 67.97 | 6.18 | 5.74 | 11.87 | 75.54 | 79.98 | 33.20 | 46.92 | 42.76 | 42.73 | | | |
| TranAD | 22.81 | 50.03 | 52.82 | 99.34 | 68.97 | 11.07 | 10.66 | 4.02 | 59.74 | 39.41 | 70.30 | 50.51 | -32.21 | -32.56 | 25.50 | 88.90 | 55.65 | 99.66 | 71.42 | 20.64 | 20.30 | | | |
| NCAD | 9.20 | 56.05 | 56.38 | 83.30 | 67.25 | 22.46 | <u>22.14</u> | 23.09 | 53.45 | 51.88 | 99.99 | 68.32 | 7.67 | 7.25 | 5.70 | 82.92 | 65.01 | 85.58 | 73.89 | 44.64 | 44.46 | | | |
| Deep IF | 19.11 | 55.94 | 51.45 | 100.0 | 67.94 | 6.08 | 5.64 | 29.14 | 60.09 | 53.75 | 98.67 | 69.59 | 14.31 | 13.93 | 21.65 | 89.52 | 52.98 | 100.0 | 69.26 | 11.64 | 11.24 | | | |
| AnomTrans | 18.39 | 52.61 | 50.21 | 99.83 | 66.81 | -4.53 | 0.83 | 16.06 | 52.18 | 55.84 | 99.11 | <u>71.44</u> | <u>16.49</u> | <u>20.90</u> | 8.27 | 80.80 | 50.24 | 99.49 | 66.77 | -10.83 | 0.96 | | | |
| TimesNet | 21.24 | 57.18 | 51.12 | 99.95 | 67.64 | 4.81 | 4.36 | 24.37 | 53.73 | 49.50 | 99.86 | 66.19 | -1.52 | -1.99 | 4.98 | 73.24 | 57.84 | 93.77 | 71.55 | 27.16 | 26.86 | | | |
| DCdetector | 11.62 | 50.31 | 51.96 | 97.77 | 67.85 | 2.52 | 7.52 | 26.56 | 58.50 | 55.55 | 99.78 | 71.37 | 15.48 | 19.97 | 8.16 | 50.68 | 52.63 | 98.30 | 68.56 | -1.28 | 10.00 | | | |
| D3R | 23.98 | 63.00 | 53.61 | 99.97 | 69.79 | 8.92 | 7.65 | 22.71 | 54.56 | 51.43 | 100.00 | 67.92 | -0.21 | 0.07 | 45.89 | 79.95 | 61.47 | 78.52 | 68.96 | 29.47 | 36.02 | | | |
| GPT2-Adapter | 13.72 | 52.03 | 53.31 | 97.01 | 68.81 | 7.80 | 6.75 | 24.12 | 55.48 | 53.28 | 99.84 | 69.48 | 7.18 | 3.67 | 1.78 | 50.00 | 52.51 | 98.13 | 68.41 | -1.79 | 0.07 | | | |
| NPSR | 23.72 | 61.16 | 52.05 | 99.81 | 68.42 | 2.89 | 7.88 | 22.68 | 38.74 | 51.46 | 100.00 | 67.95 | -0.06 | 5.68 | <u>76.88</u> | <u>90.18</u> | 71.21 | 81.16 | <u>75.86</u> | 52.54 | <u>53.73</u> | | | |
| Ours | 30.02 | <u>62.70</u> | 56.30 | 99.76 | 71.98 | <u>18.50</u> | 22.37 | 29.39 | 65.46 | 56.84 | 99.82 | 72.44 | 19.91 | 24.07 | 82.03 | 90.31 | 78.46 | 80.88 | 79.65 | 64.93 | 66.82 | | | |

| Datasets | WADI | | | | | | | | PSM | | | | | | | | NIPS-TS-Swan | | | | | | | |
|--------------|--------------|--------------|---------|---------|--------------|--------------|--------------|--------------|--------------|-------|---------|--------------|--------------|--------------|--------------|--------------|--------------|-------|--------------|--------------|--------------|---------|---------|---------|
| | F1 | AUC | Aff-Pre | Aff-Rec | Aff-F1 | UAff-F1 | NAff-F1 | NAff-F1 | F1 | AUC | Aff-Pre | Aff-Rec | Aff-F1 | UAff-F1 | NAff-F1 | NAff-F1 | F1 | AUC | Aff-Pre | Aff-Rec | Aff-F1 | UAff-F1 | NAff-F1 | NAff-F1 |
| Random | 10.79 | 50.03 | 54.81 | 99.95 | 70.79 | 0.00 | 17.54 | 40.93 | 50.16 | 53.17 | 99.95 | 69.41 | 0.00 | 11.91 | 46.25 | 50.13 | 54.83 | 96.82 | 70.01 | 0.00 | 17.56 | | | |
| Deep SVDD | 7.34 | 59.47 | 50.06 | 55.79 | 52.77 | 0.72 | 0.24 | 44.46 | 78.09 | 53.92 | 99.98 | 70.06 | 14.93 | 14.56 | <u>55.99</u> | <u>75.32</u> | 56.84 | 89.93 | 69.66 | 24.07 | 23.76 | | | |
| USAD | 10.86 | 53.61 | 54.92 | 100.0 | 70.90 | 18.27 | 17.91 | 47.90 | 64.53 | 55.30 | 98.71 | 70.88 | 19.48 | 19.14 | 52.63 | 66.76 | 55.26 | 68.62 | 61.22 | 18.57 | 18.25 | | | |
| TCN-ED | 10.86 | 53.01 | 54.92 | 100.0 | 70.90 | 18.27 | 17.91 | 43.46 | 63.97 | 53.16 | 100.00 | 69.42 | 12.29 | 11.89 | 49.22 | 71.37 | 55.10 | 99.92 | 71.03 | 18.87 | 18.52 | | | |
| COLTA | 26.92 | 50.52 | 99.18 | 23.08 | 37.44 | 37.38 | 37.38 | 0.08 | 71.45 | 100.0 | 5.12 | 9.75 | 9.75 | 0.17 | 71.38 | 69.25 | 0.10 | 0.19 | 0.19 | 0.19 | | | | |
| TranAD | 11.78 | 52.60 | 55.91 | 91.96 | 69.54 | 21.27 | 20.94 | 43.20 | 65.22 | 60.88 | 92.09 | 73.30 | 35.44 | 35.19 | 51.93 | 70.00 | 57.86 | 90.18 | 70.49 | 27.07 | 26.78 | | | |
| NCAD | 10.87 | 62.84 | 54.99 | 100.0 | 70.96 | 18.49 | 18.14 | 4.05 | 61.76 | 77.79 | 53.08 | 63.10 | <u>54.35</u> | <u>54.30</u> | 0.89 | 52.24 | 48.28 | 0.98 | 1.92 | -1.50 | -0.02 | | | |
| Deep IF | 10.86 | 51.43 | 54.92 | 100.0 | 70.90 | 18.27 | 17.91 | 43.47 | 69.06 | 53.15 | 100.00 | 69.41 | 12.24 | 11.84 | 49.19 | 73.30 | 55.10 | 99.98 | 71.05 | 18.86 | 18.51 | | | |
| AnomTrans | 6.40 | 50.80 | 51.43 | 95.15 | 66.77 | -13.84 | 5.56 | 39.81 | 52.18 | 52.78 | 96.07 | 68.13 | -1.65 | 10.51 | 44.86 | 54.62 | 55.21 | 92.36 | 69.11 | 1.68 | 18.73 | | | |
| TimesNet | 17.65 | 65.08 | 65.25 | 99.30 | 49.05 | 34.45 | 34.34 | 2.49 | 58.74 | 77.84 | 67.23 | 72.15 | 60.97 | 60.91 | 43.16 | 53.62 | 60.75 | 81.29 | 69.53 | <u>34.23</u> | <u>33.99</u> | | | |
| DCdetector | 8.27 | 50.12 | 59.72 | 94.64 | 73.23 | 19.51 | 32.26 | 22.72 | 50.38 | 53.05 | 94.98 | 68.08 | -0.49 | 11.47 | 48.83 | 50.35 | 55.08 | 99.82 | 70.99 | 1.11 | 18.45 | | | |
| D3R | 12.86 | 51.39 | 56.47 | 99.98 | 72.17 | 7.09 | 2.46 | 44.24 | 60.64 | 53.84 | 100.00 | 69.99 | 2.82 | 3.93 | 49.45 | 62.54 | 57.70 | 96.06 | 72.10 | 11.93 | 9.98 | | | |
| GPT2-Adapter | 5.59 | 50.01 | 55.62 | 98.29 | 71.04 | 3.55 | -0.27 | 35.24 | 50.74 | 54.33 | 95.16 | 69.17 | 4.84 | 2.18 | 45.23 | 58.77 | 61.17 | 69.55 | 65.09 | 23.36 | 18.28 | | | |
| NPSR | <u>50.67</u> | <u>80.19</u> | 65.15 | 90.45 | <u>75.74</u> | 36.53 | <u>45.39</u> | 51.02 | 70.67 | 54.71 | 99.37 | 70.56 | 6.29 | 17.14 | 49.30 | 62.61 | 55.13 | 99.99 | 71.07 | 1.32 | 18.61 | | | |
| Ours | 63.98 | 87.97 | 82.36 | 92.81 | 87.27 | 73.59 | 76.26 | 52.07 | 71.99 | 62.46 | 91.76 | 74.33 | 32.63 | 39.20 | 71.23 | 85.17 | 76.17 | 53.75 | 63.03 | 50.29 | 53.04 | | | |

4.5 Sensitivity analysis

We performed a sensitivity analysis on the hyperparameters of SimAD. The hyperparameters significantly affecting SimAD’s performance are the window size and the number of patch embeddings (others are listed in the appendix). Figure 3 illustrates the influence of different window sizes on the model’s performance on the WADI dataset. As the window size increases, the model’s loss exhibits a decreasing trend, and its accuracy consistently improves. A larger window size incorporates more temporal and contextual information, enabling the model to comprehensively understand data patterns and trends, thus improving detection performance. It is worth noting that when the window size increases from 1024 to 2048, the model’s loss further decreases, but the improvement in the F1 score is limited. This suggests that larger window sizes also increase the optimization difficulty.

Figure 4 depicts the impact of the number of patch embeddings on the model’s performance. When the number of patch embeddings is set to 0 (equivalent to the original attention mechanism), the model’s performance is significantly lower compared to using EmbedPatch with embedded queries. This demonstrates the superiority of our model’s performance and the effectiveness of EmbedPatch in enhancing the memory of normal samples. As the number of patch embeddings increases, the model’s Rec Loss and F1 Score exhibit fluctuating changes. Based on Figure 4, it can be inferred that the model achieves optimal performance when the number of patch embeddings is between 100 and 200.

Table 2: The average performance of different algorithms on UCR datasets.

| Metrics | Methods | UCR | | | | | |
|---------|------------|--------------|---------|---------|--------------|--------------|--------------|
| | | F1 | Aff-Pre | Aff-Rec | Aff-F1 | UAff-F1 | NAff-F1 |
| Avg.+ | AnomTrans | 1.17 | 50.66 | 98.94 | 66.88 | 9.41 | 10.88 |
| | DCdetector | 1.66 | 50.90 | 99.96 | 67.41 | 6.71 | 5.52 |
| | Ours | 14.99 | 57.83 | 99.91 | 72.52 | 35.16 | 34.38 |
| Avg. | AnomTrans | 1.15 | 50.39 | 97.73 | 66.55 | 1.30 | 1.23 |
| | DCdetector | 1.61 | 50.63 | 83.30 | 67.06 | 2.01 | 2.64 |
| | Ours | 14.99 | 57.83 | 97.47 | 72.52 | 19.53 | 19.46 |

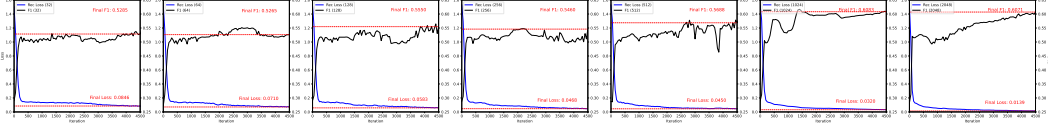


Figure 3: The impact of different window sizes on the model.

From Figure 5, it is evident that increasing the number of layers and an appropriate level of noise and model dimension can result in improved model performance. However, a notable decline in performance is observed when the model dimension is set to 128. This indicates that models with smaller dimensions face challenges in learning complex feature representations.

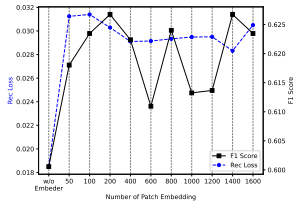


Figure 4: Different numbers of embeddings.

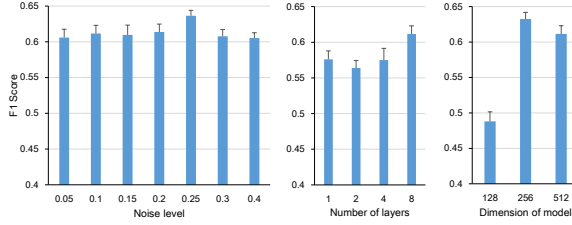


Figure 5: Other hyper-parameters. The error bar represents the standard deviation.

4.6 Ablation analysis

To validate the effectiveness and necessity of our model design, we conducted ablation studies on ContrastFusion, data augmentation, EmbedPatch, and asymmetric optimization modules on all datasets, as depicted in Figure 6.

The complete results of the ablation experiments are presented in Table 6 in the appendix. (1) **w/o Sim** represents the model without the ContrastFusion module. After removing this module, the F1 score of the model decreased by 7.88%, indicating that ContrastFusion is important for the overall performance of the model, aiding in learning distinct features to differentiate between normal and abnormal samples. (2) **w/o Aug** represents the model without the data augmentation module. Compared to the ablation of other modules, the impact of removing the data augmentation module is relatively small. However, removing it still results in a decrease of 43.69% in UAff-F1, demonstrating its ability to improve the model’s generalization. (3) **w/o Embedder** represents the model without the EmbedPatch module. It can be easily observed from the table that the ablation of this module has the most significant impact on the model’s F1 score. This indicates that incorporating EmbedPatch into the attention mechanism is crucial for the model to learn appropriate representations of temporal data. (4) **w/o Joint** represents the model without the asymmetric optimization module. The ablation of this module results in a decrease in all performance metrics, particularly a significant drop of 43.69% in NAff-F1. This suggests that asymmetric optimization helps the model focus on abnormal samples.

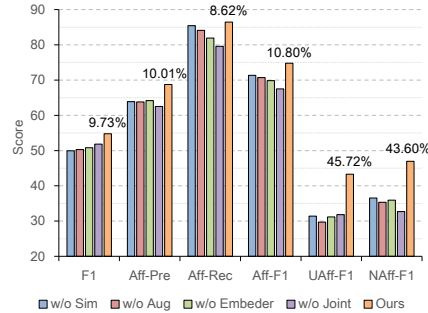


Figure 6: Ablation analysis. The data labeling serves as an upper bound on the performance improvement achievable by our enhanced model.

Additionally, Figure 7 offers a more comprehensive depiction of the training process using PSM data. It can be observed that the **w/o Embedder** model achieves the lowest loss but the lowest F1 score. The **w/o Sim** model also exhibits a similarly low loss but suffers from negative optimization, resulting in a relatively low F1 score. In contrast, SimAD, despite having a higher final loss, achieves the highest F1 score. This clearly demonstrates that optimizing solely for reconstruction is inadequate, and SimAD effectively addresses the challenges outlined in the introduction.

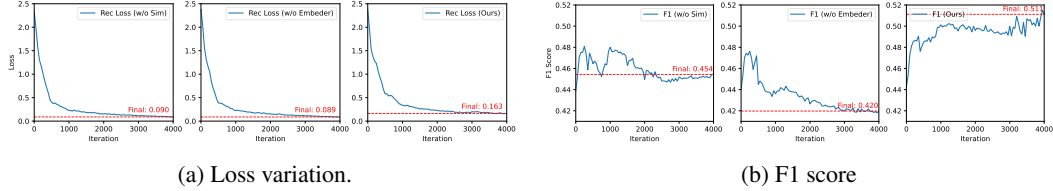


Figure 7: Loss and F1 score variations on dataset PSM.

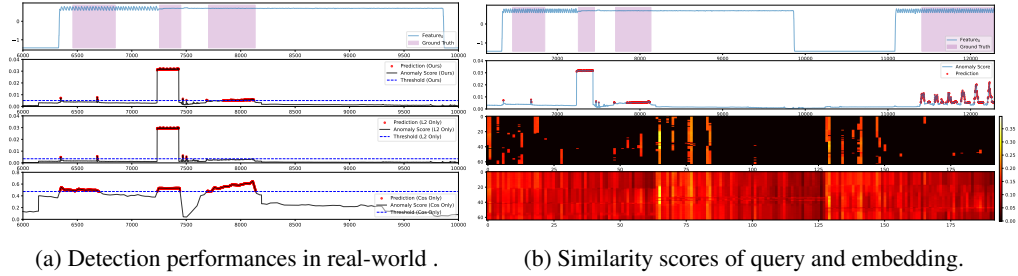


Figure 8: Real world case study on dataset SWaT.

4.7 Visualization analysis

4.7.1 Real-world cases analysis

The real performance of SimAD on the SWaT dataset is presented in Figure 8a and Figure 10 (in the appendix). The first row of images showcases the original data and the ground truth labels. The second row of images presents the predicted results of our model, which effectively detects most anomalies by assigning significantly higher scores to abnormal data than normal data. The third and fourth rows of images illustrate the results obtained using L2 loss and patch-based cosine similarity loss as anomaly scores, respectively. It is evident that the former focuses more on short-duration anomalies, while the latter can capture long-duration anomalies. In the appendix, Figure 11 presents the detection results of AnomTrans. Our method exhibits superior performance compared to AnomTrans, as it can only detect a few anomalies and encounters difficulties in accurately detecting segment anomalies. The case study highlights the effectiveness and rationale behind our anomaly score design.

4.7.2 Explanation of patch embedding

Similarly, Figure 8b illustrates the detection performance of SimAD. The fourth row of images represents the similarity between the query and the embedding of the last layer, while the third row of images displays the similarity scores between the last layer’s embedding and the top 5 most relevant queries. When combined with Figure 12 in the appendix, it can be observed that in the lower layers, the embedding establishes relationships with a majority of the queries. However, only the normal data can establish relationships with EmbedPatch in the higher layers. This indicates that in the shallow layers, SimAD learns general representations, while in the higher layers, it learns features associated with normal data, resulting in less similarity between abnormal data and EmbedPatch. Consequently, the patch embeddings enhance the detection performance of SimAD.

5 Conclusion

This paper introduces a **Simple** dissimilarity-based approach for time series **Anomaly Detection** (SimAD). The proposed framework is characterized by its simplicity and versatility, enabling longer time windows. The experimental results provide evidence of the superiority of our method compared to existing approaches. Furthermore, we present two improved evaluation metrics, UAff and NAff, which effectively assess the algorithm’s performance. In future work, we plan to extend this detection scheme to various other scenarios and strive to develop a unified model for anomaly detection.

References

- [1] Mingxuan Zhang, Yan Sun, and Faming Liang. Sparse Deep Learning for Time Series Data: Theory and Applications, 2023.
- [2] Gen Li and Jason J. Jung. Deep learning for anomaly detection in multivariate time series: Approaches, applications, and challenges. *Information Fusion*, 91:93–102, 2023.
- [3] Bedeuro Kim, Mohsen Ali Alawami, Eunsoo Kim, Sanghak Oh, Jeongyong Park, and Hyoungshick Kim. A Comparative Study of Time Series Anomaly Detection Models for Industrial Control Systems. *Sensors*, 23(3):1310, 2023.
- [4] Yuxin Zhang, Jindong Wang, Yiqiang Chen, Han Yu, and Tao Qin. Adaptive Memory Networks with Self-supervised Learning for Unsupervised Anomaly Detection. *IEEE Transactions on Knowledge and Data Engineering*, 4347(c):1–13, 2022.
- [5] Zhikang Liu, Yiming Zhou, Yuansheng Xu, and Zilei Wang. SimpleNet: A Simple Network for Image Anomaly Detection and Localization, 2023.
- [6] Zhiyuan You, Lei Cui, Yujun Shen, Kai Yang, Xin Lu, Yu Zheng, and Xinyi Le. A Unified Model for Multi-class Anomaly Detection, 2022.
- [7] Zhijie Zhong, Kaixiang Yang, Zhiwen Yu, Yifan Shi, and C L Philip Chen. Towards Efficient Anomaly Detection Using Memory Broad Learning System.
- [8] Jiehui Xu, Haixu Wu, Jianmin Wang, and Mingsheng Long. Anomaly Transformer: Time Series Anomaly Detection with Association Discrepancy. 2021.
- [9] Astha Garg, Wenyu Zhang, Jules Samaran, Ramasamy Savitha, and Chuan-Sheng Foo. An evaluation of anomaly detection and diagnosis in multivariate time series. *IEEE Transactions on Neural Networks and Learning Systems*, 33(6):2508–2517, 2021.
- [10] Siwon Kim, Kukjin Choi, Hyun-Soo Choi, Byunghan Lee, and Sungroh Yoon. Towards a Rigorous Evaluation of Time-Series Anomaly Detection. *Proceedings of the AAAI Conference on Artificial Intelligence*, 36(7):7194–7201, 2022.
- [11] Keval Doshi, Shatha Abudalou, and Yasin Yilmaz. Reward Once, Penalize Once: Rectifying Time Series Anomaly Detection. In *2022 International Joint Conference on Neural Networks (IJCNN)*, pages 1–8, 2022.
- [12] Renjie Wu and Eamonn J. Keogh. Current Time Series Anomaly Detection Benchmarks are Flawed and are Creating the Illusion of Progress (Extended Abstract). In *2022 IEEE 38th International Conference on Data Engineering (ICDE)*, pages 1479–1480, Kuala Lumpur, Malaysia, 2022. IEEE.
- [13] Lukas Ruff, Robert Vandermeulen, Nico Goernitz, Lucas Deecke, Shoaib Ahmed Siddiqui, Alexander Binder, Emmanuel Müller, and Marius Kloft. Deep one-class classification. In *International conference on machine learning*, pages 4393–4402. PMLR, 2018.
- [14] Hongzuo Xu, Guansong Pang, Yijie Wang, and Yongjun Wang. Deep isolation forest for anomaly detection. *IEEE Transactions on Knowledge and Data Engineering*, 2023.
- [15] Julien Audibert, Pietro Michiardi, Frédéric Guyard, Sébastien Marti, and Maria A. Zuluaga. USAD: UnSupervised Anomaly Detection on Multivariate Time Series. In *Proceedings of the 26th ACM SIGKDD International Conference on Knowledge Discovery & Data Mining*, pages 3395–3404, Virtual Event CA USA, 2020. ACM.
- [16] Zhiwen Tian, Ming Zhuo, Leyuan Liu, Junyi Chen, and Shijie Zhou. Anomaly detection using spatial and temporal information in multivariate time series. *Scientific Reports*, 13(1):4400, 2023.
- [17] Haixu Wu, Tengge Hu, Yong Liu, Hang Zhou, Jianmin Wang, and Mingsheng Long. Timesnet: Temporal 2d-variation modeling for general time series analysis. In *The eleventh international conference on learning representations*, 2022.
- [18] Fanyu Zeng, Mengdong Chen, Cheng Qian, Yanyang Wang, Yijun Zhou, and Wenzhong Tang. Multivariate time series anomaly detection with adversarial transformer architecture in the Internet of Things. *Future Generation Computer Systems*, 144:244–255, 2023.
- [19] Ah-Hyung Shin, Seong Tae Kim, and Gyeong-Moon Park. Time Series Anomaly Detection Using Transformer-Based GAN With Two-Step Masking. *IEEE Access*, 11:74035–74047, 2023.

- [20] Bowen Du, Xuanxuan Sun, Junchen Ye, Ke Cheng, Jingyuan Wang, and Leilei Sun. GAN-Based Anomaly Detection for Multivariate Time Series Using Polluted Training Set. *IEEE Transactions on Knowledge and Data Engineering*, pages 1–1, 2021.
- [21] Jina Kim, Hyeongwon Kang, and Pilsung Kang. Time-series anomaly detection with stacked Transformer representations and 1D convolutional network. *Engineering Applications of Artificial Intelligence*, 120:105964, 2023.
- [22] Shreshth Tuli, Giuliano Casale, and Nicholas R. Jennings. TranAD: Deep Transformer Networks for Anomaly Detection in Multivariate Time Series Data, 2022.
- [23] Hongzuo Xu, Yijie Wang, Songlei Jian, Qing Liao, Yongjun Wang, and Guansong Pang. Calibrated One-class Classification for Unsupervised Time Series Anomaly Detection, 2022.
- [24] Chris U. Carmona, François-Xavier Aubet, Valentin Flunkert, and Jan Gasthaus. Neural Contextual Anomaly Detection for Time Series, 2021.
- [25] Yiyuan Yang, Chaoli Zhang, Tian Zhou, Qingsong Wen, and Liang Sun. DCdetector: Dual Attention Contrastive Representation Learning for Time Series Anomaly Detection. Technical Report arXiv:2306.10347, arXiv, 2023.
- [26] Hao Zhou, Ke Yu, Xuan Zhang, Guanlin Wu, and Anis Yazidi. Contrastive autoencoder for anomaly detection in multivariate time series. *Information Sciences*, 610:266–280, 2022.
- [27] Theivendiram Pranavan, Terence Sim, Arulmurugan Ambikapathi, and Savitha Ramasamy. Contrastive predictive coding for Anomaly Detection in Multi-variate Time Series Data. <https://arxiv.org/abs/2202.03639v1>, 2022.
- [28] Chengsen Wang, Zirui Zhuang, Qi Qi, Jingyu Wang, Xingyu Wang, Haifeng Sun, and Jianxin Liao. Drift doesn’t matter: Dynamic decomposition with diffusion reconstruction for unstable multivariate time series anomaly detection. *Advances in Neural Information Processing Systems*, 36, 2024.
- [29] Yuhang Chen, Chaoyun Zhang, Minghua Ma, Yudong Liu, Ruomeng Ding, Bowen Li, Shilin He, Saravan Rajmohan, Qingwei Lin, and Dongmei Zhang. ImDiffusion: Imputed Diffusion Models for Multivariate Time Series Anomaly Detection, 2023.
- [30] Tian Zhou, Peisong Niu, Xue Wang, Liang Sun, and Rong Jin. One Fits All: Power General Time Series Analysis by Pretrained LM. *Advances in Neural Information Processing Systems*, 36:43322–43355, 2023.
- [31] Taesung Kim, Jinhee Kim, Yunwon Tae, Cheonbok Park, Jang-Ho Choi, and Jaegul Choo. Reversible instance normalization for accurate time-series forecasting against distribution shift. In *International Conference on Learning Representations*, 2021.
- [32] Ching Chang, Wei-Yao Wang, Wen-Chih Peng, and Tien-Fu Chen. LLM4TS: Aligning Pre-Trained LLMs as Data-Efficient Time-Series Forecasters, 2024.
- [33] Ming Jin, Shiyu Wang, Lintao Ma, Zhixuan Chu, James Y. Zhang, Xiaoming Shi, Pin-Yu Chen, Yuxuan Liang, Yuan-Fang Li, Shirui Pan, and Qingsong Wen. Time-LLM: Time Series Forecasting by Reprogramming Large Language Models, 2024.
- [34] Ting Chen, Simon Kornblith, Mohammad Norouzi, and Geoffrey Hinton. A simple framework for contrastive learning of visual representations. In *International conference on machine learning*, pages 1597–1607. PMLR, 2020.
- [35] Pascal Vincent, Hugo Larochelle, Yoshua Bengio, and Pierre-Antoine Manzagol. Extracting and composing robust features with denoising autoencoders. In *Proceedings of the 25th international conference on Machine learning*, pages 1096–1103, 2008.
- [36] Alexis Huet, Jose Manuel Navarro, and Dario Rossi. Local Evaluation of Time Series Anomaly Detection Algorithms. In *Proceedings of the 28th ACM SIGKDD Conference on Knowledge Discovery and Data Mining*, pages 635–645, 2022.
- [37] Hoang Anh Dau, Anthony Bagnall, Kaveh Kamgar, Chin-Chia Michael Yeh, Yan Zhu, Shaghayegh Gharghabi, Chotirat Ann Ratanamahatana, and Eamonn Keogh. The ucr time series archive. *IEEE/CAA Journal of Automatica Sinica*, 6(6):1293–1305, 2019.
- [38] Chih-Yu (Andrew) Lai, Fan-Keng Sun, Zhengqi Gao, Jeffrey H. Lang, and Duane Boning. Normality Score Conditioned Time Series Anomaly Detection by Point/Sequential Reconstruction. *Advances in Neural Information Processing Systems*, 36:76637–76655, 2023.

A Flaws in previous metrics

Figure 9 illustrates an artificial example of time series anomaly detection. The top row represents the true labels of the time series data. Random1, Random2, Pred1, and Pred2 denote the anomaly scores generated by two random and other algorithms. The labels ending with "PA" indicate point adjustment, where if the model predicts any part of an anomaly segment, the entire segment is considered an identified anomaly.

Random1 predicts all timestamps as anomalies, while Random2 uniformly and randomly predicts anomalies. However, both algorithms achieve high point-adjustment F1 scores (F1PA), indicating that F1PA lacks robustness in this case.

The F1 score can exhibit this issue, as it is more suitable for evaluating shorter interval anomalies (such as the last). However, its results can still be informative and provide some reference when facing non-random predictions.

Pred1 is the top-performing model among the mentioned ones. However, its Aff-F1 score is lower than that of Random1. This is because the original Aff-F1 metric does not account for false predictions. However, the enhanced UAff-F1 metric provides a better basis for comparing the performance of Pred1 and Random1. Additionally, Pred1 outperforms Pred2, although the difference in their Aff-F1 scores is small and even lower than that of Random1. In this case, the UAff-F1 metric can provide a more effective comparison between the two models, yielding scores of 0.1818 and 0.0057 for Pred1 and Pred2, respectively, while assigning lower scores to Random1 and Random2.

Based on the above analysis, we can conclude that F1 can serve as a valuable reference metric for non-random algorithms. F1PA may result in false improvements, whereas Aff-F1 lacks sufficient discriminative power and provides inaccurate evaluations for random algorithms. Ultimately, we recommend using the enhanced UAff-F1 metric for a more accurate performance assessment.

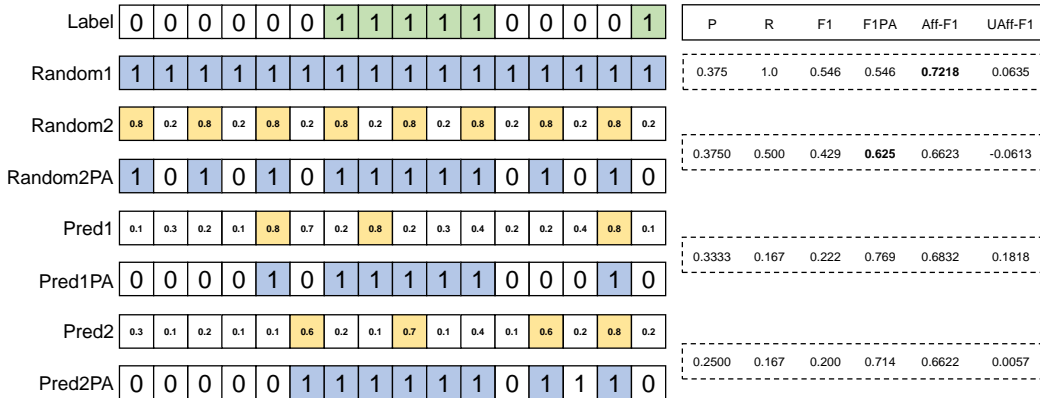


Figure 9: A case of artificial data illustrating the shortcomings of different metrics.

B Pseudo-code of SimAD

Algorithm 1 illustrates the workflow of SimAD.

C Detailed experimental settings

C.1 Baselines

We utilize official or open-source baselines that have been published on GitHub. These baselines can be downloaded by following:

1. Deep SVDD: <https://github.com/xuhongzuo/DeepOD>
2. USAD: <https://github.com/xuhongzuo/DeepOD>

Algorithm 1 SimAD training pseudo-code, Pytorch-like

```
1 # J: I.I.D GAUSSIAN NOISE
2 # FE: FEATURE EXTRACTOR
3 # ENC: EMBEDPATCH ENCODER
4 # CF: CONTRASTFUSION
5 # SIMAD: COMBINATION OF FE, ENC, AND CF
6 # R: REARRANGE DATA
7
8 for x in data_loader:
9     x1, x2 = x, x + J
10    x_out1, sim1 = SimAD(x1) # SIMAD PROCESSING
11    x_out2, sim2 = SimAD(x2)
12    # RECONSTRUCTS AND PROJECTS FEATURES
13    x_patch = R(x)
14
15    rec_loss = loss_func(x_out1, x_patch)
16    denoise_loss = loss_func(x_out2, x_patch)
17    sim_loss = loss_func(sim1, sim2.detach()) + loss_func(
18        sim2, sim1.detach())
19    loss = rec_loss + denoise_loss - sim_loss * warmup
20    loss.backward()
21
22    update(SimAD)
23
24 # LOSS FUNCTION
25 def loss_func(s1, s2):
26     return l2_loss(s1, s2) + (1 - cos_loss(s1, s2)).mean()
```

3. TCN-ED: <https://github.com/xuhongzuo/DeepOD>
4. COUTA: <https://github.com/xuhongzuo/DeepOD>
5. TranAD: <https://github.com/xuhongzuo/DeepOD>
6. NCAD: <https://github.com/xuhongzuo/DeepOD>
7. Deep IF: <https://github.com/xuhongzuo/DeepOD>
8. AnomTrans: <https://github.com/thuml/Anomaly-Transformer>
9. TimesNet: <https://github.com/xuhongzuo/DeepOD>
10. DCdetector: <https://github.com/DAMO-DI-ML/KDD2023-DCdetector/>
11. D3R: <https://github.com/ForestsKing/D3R/>
12. GPT2-Adapter: https://github.com/PSacfc/GPT4TS_Adapter
13. NPSR: <https://github.com/andrewlai61616/NPSR/>

C.2 Datasets details

Existing methods extensively utilize many publicly available real-world datasets. We evaluate model performance using six multivariate datasets: (1) MSL (Mars Science Laboratory dataset), (2) SMAP (Soil Moisture Active Passive dataset), (3) SWaT (Secure Water Treatment Testbed), (4) WADI (Water Distribution Testbed), (5) PSM (Pooled Server Metrics), and (6) Swan. The details are provided in Table 4.

They can be downloaded in:

- MSL & SMAP: <https://github.com/ML4ITS/mtad-gat-pytorch>
- SWaT: https://itrust.sutd.edu.sg/itrust-labs_datasets
- WADI: <https://itrust.sutd.edu.sg/testbeds/water-distribution-wadi>

- UCR: https://www.cs.ucr.edu/~eamonn/time_series_data_2018/UCR_TimeSeriesAnomalyDatasets2021.zip
- Others: <https://github.com/DAMO-DI-ML/KDD2023-DCdetector>.

Table 4: Details of benchmark datasets.

| Dataset | #Training | #Test (Labeled) | Dimension | Anomaly ratio (%) | Bias | Ideal Bias |
|---------|-----------|-----------------|-----------|-------------------|-------|------------|
| MSL | 58317 | 73729 | 55 | 10.5 | 51.34 | 50.55 |
| SMAP | 135183 | 427617 | 25 | 12.8 | 51.48 | 50.82 |
| SWaT | 99000 | 89984 | 26 | 12.2 | 52.94 | 50.74 |
| WADI | 1048571 | 172801 | 123 | 5.99 | 54.81 | 50.18 |
| PSM | 132481 | 87841 | 25 | 27.8 | 53.17 | 53.86 |
| Swan | 60000 | 60000 | 38 | 32.6 | 54.83 | 55.31 |

C.3 Implementation details

In our default configuration, we set the length of the sliding window to 2048. The patch size is 32. The model is configured with a hidden dimension of 512, 8 attention heads, and 8 layers. We utilize 1000 embedding features. For all methods, we use the optimal F1 search strategy. The training process employs the AdamW optimizer with a batch size 256 and a learning rate of 10^{-3} . We also utilize cosine learning rate scheduling. The training is conducted over 20 epochs, with each epoch randomly sampling 500 samples. Our algorithm is implemented in Python using PyTorch. All experiments were performed on an NVIDIA A800 (80GB) GPU.

C.4 Bias data of Affiliation precision

Table 4 presents various datasets’ actual and ideal biases. The theoretical ideal bias is determined by assuming the presence of only one anomaly segment in the test data, considering the anomaly rate and theoretical analysis from [36]. It is worth noting that the disparity between the two biases falls within an acceptable range. Hence, in practical scenarios where obtaining the true bias is challenging, the UAff metric can still be computed by estimating the anomaly ratio and calculating the theoretical bias.

$$\mathbf{Bias}_{ideal} = \frac{1}{2} + \frac{1}{2} \cdot (\text{AnomalyRatio})^2 \quad (11)$$

D Mathematical analysis of UAff and NAff metrics

D.1 Range analysis

Since NAff is a specific case of UAff, we will begin by analyzing UAff. To keep it concise, we will use the following abbreviations: **naff** for NAff-F1, **uap** for NAff-Pre, **ap** for Aff-Pre, **ar** for Aff-Rec, and **ap_b** for Aff-Pre_{bias}.

Thus, we have $\mathbf{naff} = \frac{\mathbf{ap} - \mathbf{ap}_b}{1 - \mathbf{ap}_b}$. Moreover, it is theoretically true that **ap** and **ap_b** are both within the range of [0, 1]. Next, we proceed to calculate the partial derivatives of **uap** concerning **ap** and **ap_b**.

$$\frac{\partial \mathbf{uap}}{\partial \mathbf{ap}} = \frac{1}{1 - \mathbf{ap}_b} \geq 0 \quad (12)$$

$$\frac{\partial \mathbf{uap}}{\partial \mathbf{ap}_b} = \frac{\mathbf{ap} - 1}{(1 - \mathbf{ap}_b)^2} \leq 0 \quad (13)$$

Based on the formulas above, it can be observed that **uap** exhibits a monotonic increase with **ap** and a monotonic decrease with **ap_b**. Consequently, when **ap** = 1, **uap** attains its maximum value of 1. In the scenario where **ap** = 0 and **ap_b** = 1, **uap** approaches a minimum limit of $-\infty$.

Nevertheless, as concluded in [36], $\mathbf{ap}_b = 1$ is applicable only when all the data points are anomalies. Generally, the proportion of anomalies in most datasets is typically below 0.5. Hence, it follows that $\mathbf{ap}_b < \frac{1}{2} + \frac{1}{2} \times 0.5^2 = 0.6125$. Furthermore, the minimum value of \mathbf{ap}_b tends to approach 0.5. However, given that \mathbf{ap}_b is derived from simulated calculations, we propose a more lenient condition of $\mathbf{ap}_b > 0.4$. Consequently, in practical scenarios, the range for \mathbf{ap}_b becomes broader, specifically $\mathbf{ap}_b \in (0.4, 0.6125)$.

Based on Eq.(13), in the scenario where $\mathbf{ap} = 0$ and $\mathbf{ap}_b \rightarrow 0.6125$, \mathbf{uap} tends towards $\frac{0-0.6125}{1-0.6125} = -1.587$. Therefore, it can be concluded that \mathbf{uap} falls within the range of $(-1.587, 1]$.

Let's proceed with analysing \mathbf{uaf} next. Given that \mathbf{ar} falls within the range of $[0, 1]$, as indicated by Equation (10), it becomes evident that when \mathbf{uap} is within the range of $[0, 1]$, the maximum value of \mathbf{uaf} is 1. In the case where \mathbf{ap}_b falls within the interval of $(-1.587, 0)$, it becomes necessary to determine the minimum value of \mathbf{uaf} . This problem can be reformulated as the search for the corresponding values of \mathbf{ap}_b within the range of $(0, 1.587)$ that yield the maximum value of \mathbf{uaf} .

The minimum value of \mathbf{uaf} can be calculated as $-\frac{2 \times 1.587 \times 1}{1.587 + 1} = -1.227$. Consequently, the range of **UAff-F1** is $(-1.227, 1]$. Based on the above analysis, it can be concluded that the range of **NAff-F1** is $[-1, 1]$ since it is a specific case of **UAff-F1**.

D.2 Distinctiveness of metrics

It can be briefly analyzed that UAff offers greater discrimination than the original Aff metric. The design intention is to ensure that the ratio of UAff to Aff, $\frac{\mathbf{uap}}{\mathbf{ap}}$, is always greater than 1 or less than 1 in the case of equal Aff-Pre. In this case, the ratio depends solely on Aff-Pre. Therefore, the problem can be reformulated as proving: $\frac{\mathbf{uap}}{\mathbf{ap}} \geq 1$ or $\frac{\mathbf{uap}}{\mathbf{ap}} \leq 1$.

By calculating the partial derivative of $\mathcal{D} = \frac{\mathbf{uap}}{\mathbf{ap}} = \frac{\mathbf{ap} - \mathbf{ap}_b}{\mathbf{ap}(1 - \mathbf{ap}_b)}$ with respect to \mathbf{ap} , we obtain:

$$\frac{\partial \mathcal{D}}{\partial \mathbf{ap}} = \frac{\mathbf{ap}_b(1 - \mathbf{ap})}{1 - \mathbf{ap}_b} \geq 0. \quad (14)$$

Hence, when $\mathbf{ap} = 1$, $\mathcal{D}_{max} = 1$, indicating that $\mathcal{D} \leq 1$, which aligns with our objective.

Based on the results presented in Table 1, it is evident that the random algorithm attains the 6th position in Aff-F1, whereas it only achieves the 13th and 9th positions in UAff-F1 and NAff-F1, respectively. This observation highlights that the enhanced metrics can provide a more precise evaluation of the algorithm's actual performance. The rankings strongly suggest that the UAff-F1 and NAff-F1 metrics offer a superior assessment of the algorithm's performance compared to the original Aff-F1 metric.

E Detailed results of experiments

Table 5 presents the performance of three models, namely SimAD, AnomTrans, and DCdetector, on the UCR dataset. Considering the overall performance across all sub-datasets, it is evident that the SimAD model consistently achieves higher F1 scores compared to the baseline models. Additionally, the SimAD model for anomaly detection demonstrates the highest number of datasets with positive evaluation scores. By excluding datasets with negative evaluation scores, SimAD exhibits significantly higher composite scores for all evaluation metrics than the other baseline models. These findings indicate that SimAD can detect a wider range of anomalies. The specific results of the ablation experiments are presented in Table 6.

E.1 Additional visualization analysis

Figure 10 demonstrates the impact of different loss functions on the predicted results, threshold values, and anomaly scores. The figure shows that our model's performance is enhanced when both the L2 and cosine loss functions are employed, as compared to using either the L2 loss function alone or the cosine loss function alone.

Table 5: Comparison results on UCR datasets.

| Datasets | | UCR | | | | | |
|----------|------------|-------|---------|---------|--------|---------|---------|
| Metrics | Methods | F1 | Aff-Pre | Aff-Rec | Aff-F1 | UAff-F1 | NAff-F1 |
| Count | AnomTrans | 147 | 244 | 244 | 244 | 141 | 148 |
| | DCdetector | 149 | 206 | 206 | 206 | 127 | 144 |
| | Ours | 240 | 240 | 240 | 240 | 173 | 177 |
| Avg.+ | AnomTrans | 1.17 | 50.66 | 98.94 | 66.88 | 9.41 | 10.88 |
| | DCdetector | 1.66 | 50.90 | 99.96 | 67.41 | 6.71 | 5.52 |
| | Ours | 14.99 | 57.83 | 99.91 | 72.52 | 35.16 | 34.38 |
| Avg. | AnomTrans | 1.15 | 50.39 | 97.73 | 66.55 | 1.30 | 1.23 |
| | DCdetector | 1.61 | 50.63 | 83.30 | 67.06 | 2.01 | 2.64 |
| | Ours | 14.99 | 57.83 | 97.47 | 72.52 | 19.53 | 1.00 |

Table 6: Full ablation results.

| Datasets | MSL | | | | | | SMAP | | | | | | SWaT | | | | | |
|-------------|------------|-------|---------|---------|--------|---------|---------|-------|---------|---------|--------|---------|---------|-------|---------|---------|--------|---------|
| | Variations | F1 | Aff-Pre | Aff-Rec | Aff-F1 | UAff-F1 | NAff-F1 | F1 | Aff-Pre | Aff-Rec | Aff-F1 | UAff-F1 | NAff-F1 | F1 | Aff-Pre | Aff-Rec | Aff-F1 | UAff-F1 |
| w/o Sim | 23.90 | 54.13 | 99.08 | 70.01 | 10.84 | 15.23 | 22.56 | 51.94 | 99.86 | 68.34 | 1.89 | 7.47 | 80.31 | 77.66 | 76.52 | 77.09 | 62.29 | 64.21 |
| w/o Aug | 29.07 | 54.64 | 98.88 | 70.39 | 12.72 | 16.98 | 23.78 | 52.66 | 98.11 | 68.53 | 4.75 | 10.09 | 79.14 | 80.60 | 64.14 | 71.43 | 61.34 | 62.63 |
| w/o Embeder | 27.20 | 54.12 | 98.85 | 69.94 | 10.80 | 15.20 | 17.89 | 50.04 | 99.64 | 66.62 | -5.76 | 0.15 | 80.31 | 77.66 | 76.52 | 77.09 | 62.29 | 64.21 |
| w/o Joint | 28.23 | 54.13 | 98.94 | 69.98 | 10.86 | 15.25 | 22.39 | 51.46 | 99.77 | 67.90 | -0.05 | 5.69 | 82.01 | 77.35 | 83.37 | 80.25 | 63.95 | 66.06 |
| Ours | 30.02 | 56.30 | 99.76 | 71.98 | 18.50 | 22.37 | 29.39 | 56.84 | 99.82 | 72.44 | 19.91 | 24.07 | 82.03 | 78.46 | 80.88 | 79.65 | 64.93 | 66.82 |

| Datasets | WADI | | | | | | PSM | | | | | | NIPS-TS-Swan | | | | | |
|-------------|------------|-------|---------|---------|--------|---------|---------|-------|---------|---------|--------|---------|--------------|-------|---------|---------|--------|---------|
| | Variations | F1 | Aff-Pre | Aff-Rec | Aff-F1 | UAff-F1 | NAff-F1 | F1 | Aff-Pre | Aff-Rec | Aff-F1 | UAff-F1 | NAff-F1 | F1 | Aff-Pre | Aff-Rec | Aff-F1 | UAff-F1 |
| w/o Sim | 62.68 | 70.55 | 84.04 | 76.71 | 49.26 | 55.20 | 45.78 | 58.83 | 96.05 | 72.96 | 21.47 | 29.83 | 64.34 | 70.24 | 57.00 | 62.93 | 42.69 | 47.34 |
| w/o Aug | 63.19 | 75.92 | 81.53 | 78.63 | 59.40 | 63.38 | 41.79 | 56.43 | 96.15 | 71.12 | 12.98 | 22.67 | 64.83 | 62.55 | 65.81 | 64.14 | 27.13 | 36.34 |
| w/o Embeder | 61.36 | 70.73 | 59.61 | 64.70 | 44.29 | 48.91 | 49.78 | 61.47 | 94.80 | 74.58 | 29.86 | 36.93 | 68.32 | 71.04 | 62.03 | 66.23 | 45.47 | 50.14 |
| w/o Joint | 56.89 | 63.33 | 63.98 | 63.65 | 56.26 | 37.64 | 52.26 | 59.93 | 91.27 | 72.35 | 24.93 | 32.62 | 69.14 | 68.85 | 40.28 | 50.82 | 35.06 | 38.95 |
| Ours | 63.98 | 82.36 | 92.81 | 87.27 | 73.59 | 76.26 | 52.07 | 62.46 | 91.76 | 74.33 | 32.63 | 39.20 | 71.23 | 76.17 | 53.75 | 63.03 | 50.29 | 53.04 |

Figure 11 illustrates the actual detection performance of the AnomTrans and NPSR on the SWaT dataset. AnomTrans can only detect a few anomalies. In Case 1, two anomalies were not detected and AnomTrans struggled with accurately detecting segment anomalies. Moreover, the anomaly score differentiation is relatively low, as in Case 2, where it has limited success detecting anomalies. In cases 3 and 4, NPSR is more effective in detecting anomalies than AnomTrans, especially segment anomalies. However, NPSR fails to detect certain anomalies, such as near time points 6500 and 8000. Additionally, NPSR tends to produce more false positives, as observed around time point 140000, where a few instances are falsely classified as positive. Furthermore, Figure 12 illustrates the similarity scores at various model layers. In the initial layer, the similarity scores exhibit a relatively dispersed pattern. However, as the number of layers increases, the similarity scores gradually rise, leading to more focused attention.

F Time costs

Table 7 presents a comparative analysis of SimAD and other models regarding model size, training time, and testing time using the SWaT dataset. The estimated training time for all methods involved training on 128,000 samples to ensure a fair comparison. However, an issue with the original code of the D3R model caused its reported testing time to be excessively long (2794.25s). To provide a more accurate estimation, we estimated the actual testing time of D3R to be 15.98s.

In terms of model size, SimAD demonstrates a significant advantage over D3R and GP2-Adapter (LLM model). Its smaller model size indicates efficient memory usage. SimAD also performs

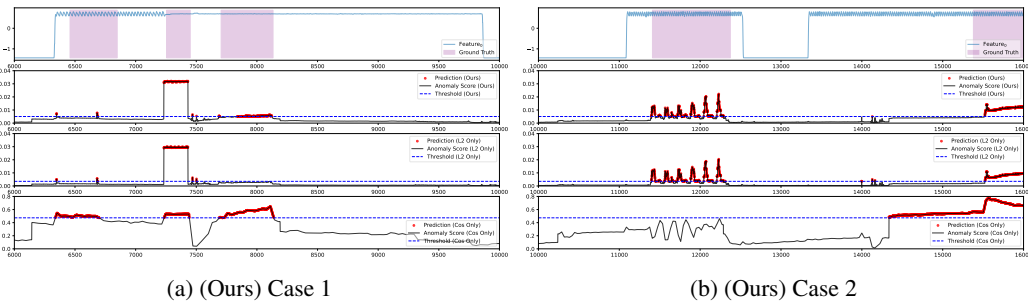


Figure 10: SimAD’s detection performances in real-world.

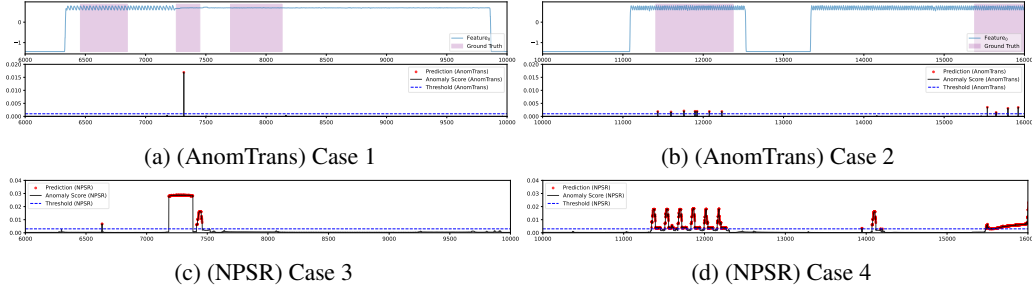


Figure 11: Other algorithms' detection performances in real-world.

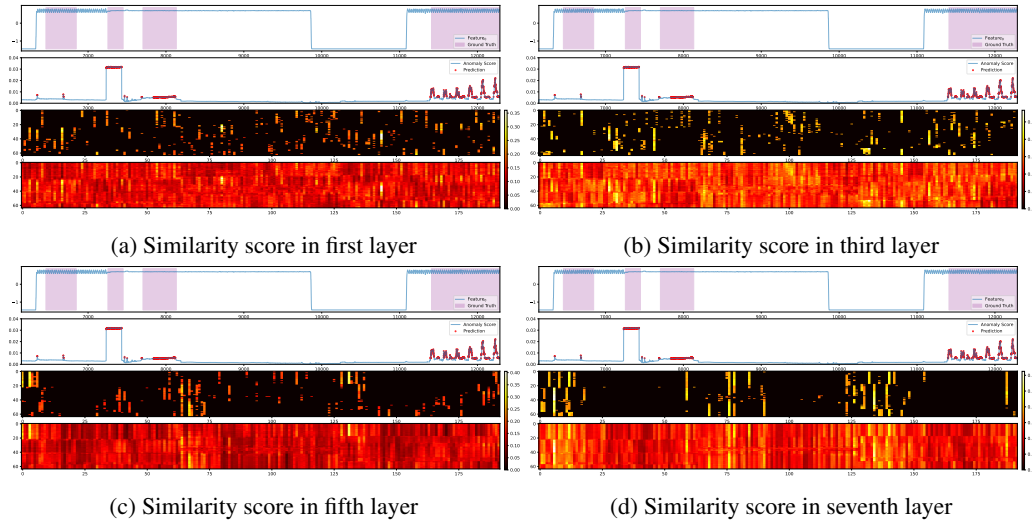


Figure 12: Similarity scores in different layers.

well regarding inference time, showing shorter inference times than other models. This implies that SimAD can make predictions faster during deployment, which can be crucial in real-time applications.

However, it's important to note that SimAD has a longer training time and a larger model size than the other models in the analysis. Despite this, considering that SimAD achieves performance improvements of over 60%, the model size and inference speed of SimAD are still within an acceptable range. To further improve SimAD, future work will explore model optimization techniques to reduce the model size while maintaining or enhancing its performance. This would address the longer training time and larger model size, making SimAD even more efficient and practical for deployment.

Table 7: The time costs of different algorithms. The lower is better.

| Methods | Model Size (MB) | Train (sec) | Test (sec) |
|--------------|-----------------|-------------|-----------------|
| USAD | 332.07 | 72.14 | 1.51 |
| TCN-ED | 0.04 | 41.34 | 0.86 |
| NCAD | 0.19 | 141.73 | 1.77 |
| AnomTrans | 28.29 | 33.25 | 3.91 |
| TimesNet | 19.15 | 24.29 | 3.62 |
| D3R | 225.10 | 1900.37 | 15.98 (2794.25) |
| GPT2-Adapter | 241.58 | 241.58 | 71.24 |
| Ours | 114.75 | 245.88 | 1.27 |

G Boader impacts

Time series anomaly detection is crucial in identifying abnormal behaviours and events. Its applications span across various domains, including risk prevention, health monitoring, and industrial inspection. The demand for effective anomaly detection techniques is high due to its wide industrial coverage. In practical scenarios, labeled data for anomalous events is often scarce. However, our method is designed to adapt to this situation and provide highly accurate detection results. There are scenarios where the model needs to perform well under resource-constrained conditions. Therefore, it becomes necessary for our model to incorporate other techniques that can reduce its size and enable it to adapt to such situations. In the future, we aspire to address this limitation by considering the model lightweight while ensuring detection accuracy, thereby creating greater societal value.

H Limitations

Significant computational costs are incurred due to the adoption of a Transformer-like architecture as the backbone of the model. In the future, we will explore alternative network frameworks, such as MAMBA or convolutional networks, that are more lightweight and efficient. Furthermore, considering the existing limitations of current time series anomaly detection algorithms, such as inaccurate evaluation and lengthy computation, we aim to propose novel evaluation metrics that are both accurate and efficient for anomaly detection.